AIP | Review of Scientific Instruments

Combinatorial thin film composition mapping using three dimensional deposition profiles

Santosh K. Suram, Lan Zhou, Natalie Becerra-Stasiewicz, Kevin Kan, Ryan J. R. Jones, Brian M. Kendrick, and John M. Gregoire

Citation: Review of Scientific Instruments **86**, 033904 (2015); doi: 10.1063/1.4914466
View online: http://dx.doi.org/10.1063/1.4914466
View Table of Contents: http://scitation.aip.org/content/aip/journal/rsi/86/3?ver=pdfcov
Published by the AIP Publishing

Combinatorial thin film composition mapping using three dimensional deposition profiles

Santosh K. Suram,[1] Lan Zhou,[1] Natalie Becerra-Stasiewicz,[1] Kevin Kan,[1]
Ryan J. R. Jones,[1] Brian M. Kendrick,[2] and John M. Gregoire[1,a)]
[1]*Joint Center for Artificial Photosynthesis, California Institute of Technology, Pasadena, California 91125, USA*
[2]*Process Equipment Division, Kurt J Lesker Company, Clairton, Pennsylvania 15025, USA*

(Received 28 January 2015; accepted 26 February 2015; published online 17 March 2015)

Many next-generation technologies are limited by material performance, leading to increased interest in the discovery of advanced materials using combinatorial synthesis, characterization, and screening. Several combinatorial synthesis techniques, such as solution based methods, advanced manufacturing, and physical vapor deposition, are currently being employed for various applications. In particular, combinatorial magnetron sputtering is a versatile technique that provides synthesis of high-quality thin film composition libraries. Spatially addressing the composition of these thin films generally requires elemental quantification measurements using techniques such as energy-dispersive X-ray spectroscopy or X-ray fluorescence spectroscopy. Since these measurements are performed *ex-situ* and post-deposition, they are unable to provide real-time design of experiments, a capability that is required for rapid synthesis of a specific composition library. By using three quartz crystal monitors attached to a stage with translational and rotational degrees of freedom, we measure three-dimensional deposition profiles of deposition sources whose tilt with respect to the substrate is robotically controlled. We exhibit the utility of deposition profiles and tilt control to optimize the deposition geometry for specific combinatorial synthesis experiments. © *2015 AIP Publishing LLC.* [http://dx.doi.org/10.1063/1.4914466]

I. INTRODUCTION

Combinatorial synthesis is currently employed for rapid discovery of materials for various applications such as photovoltaics, solar fuels, fuel cells, magnetic materials, and polymers.[1–5] Techniques for the synthesis of combinatorial libraries of materials include solution based methods,[6] advanced manufacturing, and physical vapor deposition.[7–12] Among these techniques, combinatorial sputtering provides an opportunity to carefully tune the properties of materials using various parameters such as source voltage, gas pressure, reactive gases, and deposition geometry, making this technique particularly amenable to synthesis of carefully designed, high-quality composition libraries.

Combinatorial sputtering techniques that employ multiple deposition sources typically produce a thin film whose composition varies as a function of substrate position. The use of robotically controlled deposition masks has been successfully deployed to control deposition gradients, providing custom designed composition profiles across the library substrate.[13–15] While this deposition strategy is suitable for certain applications, its implementation significantly lowers synthesis throughput and requires care to ensure intimate mixing of sequentially deposited layers. Sputter co-deposition ensures intimate mixing of the library constituents and is very efficient in its utilization of a large fraction of the material sputtered from the deposition sources. For co-deposition, sputtering parameters such as deposition atmosphere and source power are typically chosen to attain the desired chemistry and deposition rate. As a result, the desired deposition gradient from each source, and by extension the composition variation in the deposited thin film, can be tailored by controlling the deposition geometry. In particular, the distance and angle between the substrate and each deposition source strongly influence the thin film composition library resulting from co-deposition. For the related technique of pulsed laser deposition, establishing deposition profile models has enabled the calculation of composition profiles in combinatorial libraries.[16]

As applied to the determination of composition across a co-sputtered library, the speed and accuracy of deposition profiling techniques must be compared with *ex-situ* composition measurements of each co-sputtered thin film. Performing a series of co-depositions and composition measurements is a direct but costly approach for determining the deposition geometry that yields a particular composition library. As an alternative to experimental approaches, modelling the composition of a co-deposited thin film may also provide efficient design of experiments. While Monte Carlo (MC) methods have been developed to simulate deposition profiles from particular sputtering geometries,[17] these models are computationally expensive and rely on accurate construction of interatomic potentials. Continuum models are much faster and have been applied for modeling deposition profiles at a wide range of gun-tilts, deposition powers, and shadowing effects due to gun chimneys.[18] Still, important discrepancies from standard models can arise due to experimental subtleties

a)Electronic mail: gregoire@caltech.edu

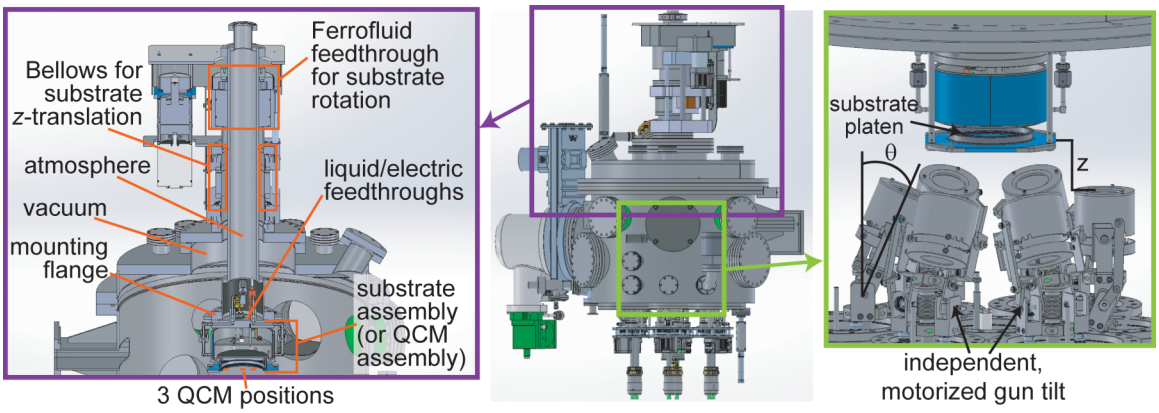

FIG. 1. Schematic of the Kurt J. Lesker CMS-24 physical vapor deposition system: (center) external view of entire chamber, (left) inset showing a cross-section view of the substrate platen with rotation and translation motion and a feedthrough flange onto which either the substrate platen or QCM platen can be mounted, (right) inset showing the in-vacuum view of 6 on-axis magnetron sources and substrate platen.

such as the surface profile of the sputter target and alterations to the magnetic field of a source due to its proximity to other sources. The experimental mapping of deposition profiles provides direct observation of the net result of these complex phenomena, motivating the measurement of deposition profiles as a function of substrate distance and angle with respect to each deposition source. A quartz crystal microbalance (QCM) can effectively measure the deposition rate from a given source at a single location within the deposition chamber, and the deposition profile of a source can be mapped using either an array of QCMs or spatial rastering of a QCM. One-dimensional motion of a QCM has been used to estimate the deposition profile from a single source in a system with fixed deposition geometry.[19] In the present work, we describe a system with robotic control of the substrate height and tilt angles of six deposition sources. This versatility in deposition geometry is coupled with a new, powerful deposition profiling technique. Three radially displaced QCMs are placed on a platen the same size as the substrate. Rastering of the QCMs through the deposition region is attained through rotation and vertical translation of the platen, enabling automated mapping of the full three-dimensional deposition rate profile. We demonstrate the utility of these deposition profiles for combinatorial co-deposition through the design of 2 ternary composition libraries: (a) a ternary composition library with maximal composition variation and (b) alloying of a tertiary element into a binary composition space.

The 3-D deposition profiling technique can be used to build a library of deposition profiles for different sources, elemental targets, and deposition geometries, from which deposition experiments can be designed. Given a complete map of the deposition profiles for a set of sources, the composition map of a co-sputtered film can be calculated under the

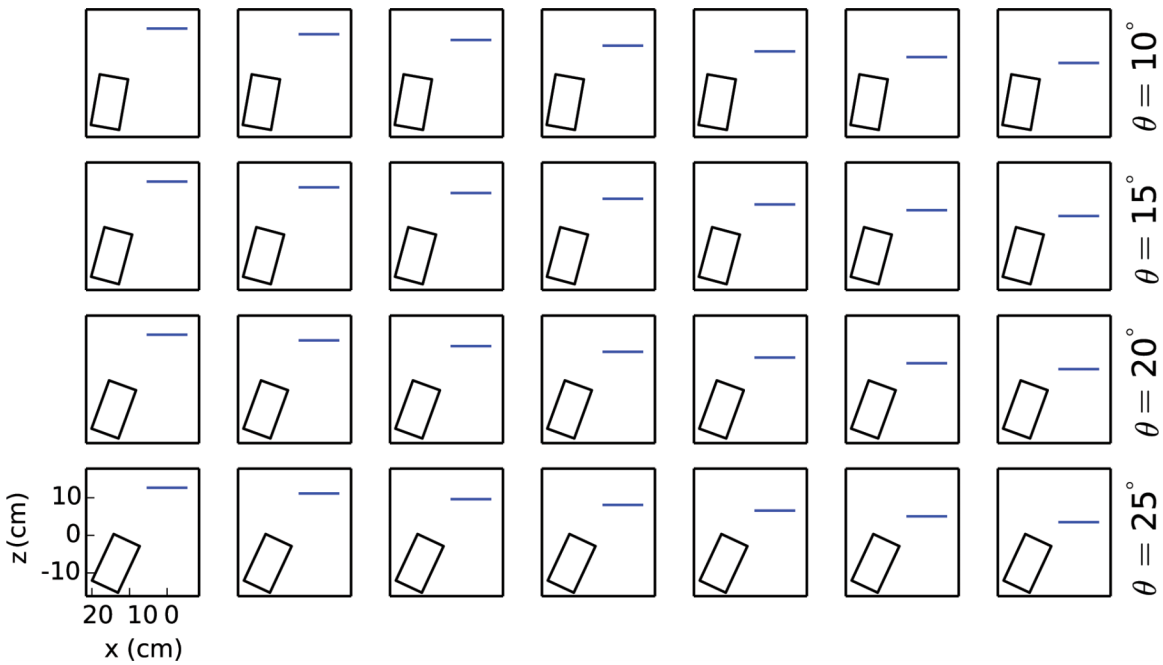

FIG. 2. A schematic showing 28 deposition geometries corresponding to four different source tilt values (θ = 10°, 15°, 20°, 25°) and seven z values (ranging from z = 3.5 to 12.6 cm). The source is depicted by a tilted rectangle, and the cross-section of a 100 mm-substrate is represented by a solid blue line.

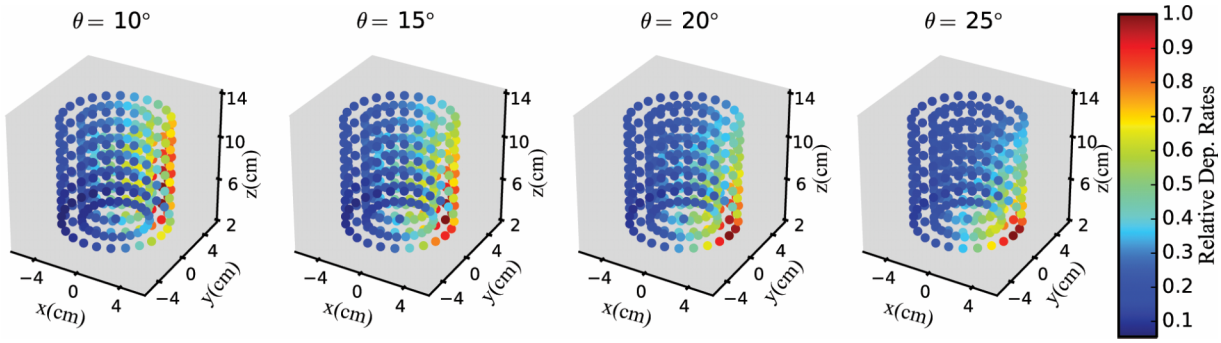

FIG. 3. Three-dimensional deposition profiles at various source tilts of 10°, 15°, 20°, and 25°. The false color scale is common to all figures and maps the deposition rates (relative to the maximum) of Cu at 60 W DC power, 360 V DC bias, and 0.8 Pa Ar.

approximation that the sticking coefficient of each element is the same in single-source and multi-source depositions. Significant deviations from this approximation occur for select combinations of co-deposited elements through resputtering processes.[20,21] During co-deposition, resputtering processes alter the effective sticking coefficient of each element, leading to deviations in composition from that calculated using the measured rates of individual sources, for which corrective models have been developed.[20,21] Advances in characterization of energetic particles in sputter deposition[22] may lead to improved models, and for the purposes of the present manuscript, we do not employ resputtering calculations.

II. EXPERIMENTAL

A. Sputter deposition system

Figure 1 shows a schematic of the combinatorial PVD system (Kurt J. Lesker, Clairton, PA) equipped with 6 on-axis magnetron sources. The substrate holder assembly is equipped with a boron nitride (BN) coated graphite serpentine filament for high-temperature depositions, and the entire substrate platen assembly is mounted on a motorized stage. The custom motion and feedthrough assembly were provided by Kurt J. Lesker, and as shown in the left inset of Figure 1, the assembly is mounted on the chamber lid. The z-motion to control the substrate height with respect to the deposition sources is enabled by linear bellows. On the top flange of the bellows, the motorized rotation is enabled by a ferrofluid rotary feedthrough which holds a tube. The inside of this tube remains at atmosphere and is terminated by a 6 in. vacuum flange labelled "mounting flange" in Figure 1. The flange that mates to the mounting flange contains the substrate platen assembly, including electrical and liquid feedthroughs. The substrate platen holds 100 mm substrates for thin film deposition, and in the present work, we describe the mapping of deposition profiles for various substrate-deposition source geometries.

To map deposition profiles, the flange containing the substrate platen assembly is removed and replaced by a flange containing the crystal monitor assembly. This assembly contains three 6 MHz Au-coated quartz crystals, each mounted in a water-cooled Inficon SL-A crystal holder. The 3 QCMs share a common water cooling line, and the corresponding liquid feedthroughs, as well as the coaxial SubMiniature version A (SMA) feedthrough for each QCM, are housed in the feedthrough flange that mates to the mounting flange. The crystals are coplanar with the substrate in the substrate platen and are positioned at the equivalent substrate locations of 0 mm, 28 mm, and 45 mm from substrate center. Radius zero corresponds to the central axis of the chamber, which is also the substrate rotation axis. It is worth noting that interchanging the substrate platen assembly and QCM assembly requires substantial effort. In practical operation, a series of deposition profiling experiments are performed with the QCM assembly, followed by a series of thin film deposition experiments with the substrate assembly.

Fig. 1 also shows a detailed view of the ensemble of 6 sputter deposition sources (2 in. Kurt J. Lesker Torus magnetrons). Each source is configured with independent, motorized tilt control so that the sputter target can be displaced by a tilt angle θ with respect to the plane of the substrate and QCMs. The position of the substrate and QCM plane is measured as z, the vertical displacement from the plane defined by the top surface of the sputter targets (when they are at tilt θ = 0°).

B. Deposition profile measurements

The deposition profiling measurements were performed using a 99.95% pure Cu target (ACI Alloys) placed in a direct

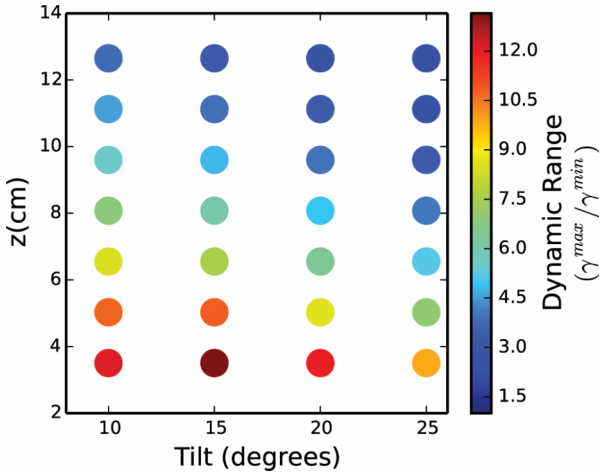

FIG. 4. A plot of the dynamic range of γ as a function of θ and z obtained from deposition profiles.

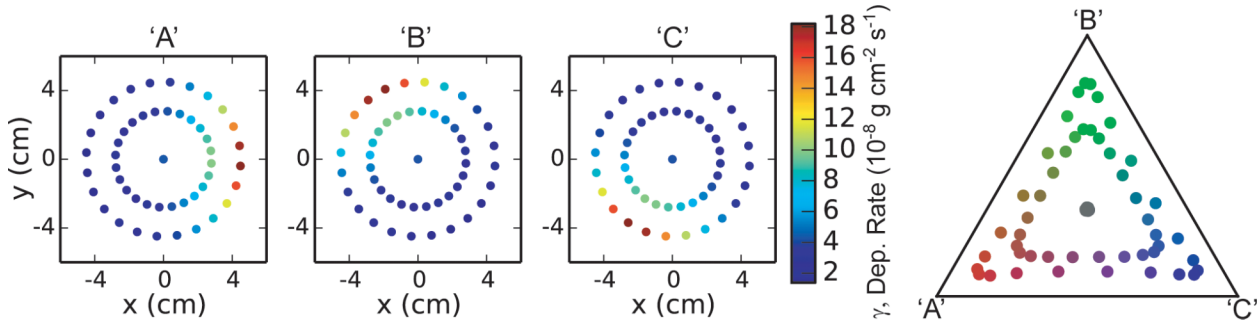

FIG. 5. Deposition rates of Cu at 60 W DC power and 0.8 Pa Ar from three sources placed at an in-plane angle of 120° relative to each other. The deposition geometry is chosen to maximize dynamic range of deposition rates (θ = 15° and z = 3.5 cm). The resulting compositions of the 49 measurement locations are shown in the right-most figure, demonstrating composition variation from 8% to 82% for each element.

current (DC) powered magnetron source and operated at a fixed power of 60 W. A base pressure of less than 6.7×10^{-6} Pa was maintained prior to the depositions using a helium cryo-pump. Depositions were carried out using Ar gas at 0.8 Pa. The deposition rates at the three QCMs were measured at four different source tilts (θ) of 10°, 15°, 20°, and 25° from the vertical. For each θ, measurements were acquired at 7 equally spaced z-heights of the crystals from 3.5 cm to 12.6 cm. Further, at each θ and z, the QCM stage was rotated from 0° to 345° at an interval of 15°, resulting in a total of 2016 deposition rate measurements that cover 28 unique geometric relationships between the deposition source and substrate. The substrate-source geometries for various values of θ and z are schematically depicted in Fig. 2.

While a planar substrate has an effective acceptance angle of 90° with respect to substrate normal, the acceptance angle of the QCMs is 78° and could lead to some shadowing of the incident sputter flux and off-center deposition of the film on the crystal. We confirmed that these phenomena are negligible for the purpose of deposition profiling by measuring the deposition rate at the most oblique deposition geometry and comparing it to the thickness of a film deposited in this geometry; the results agreed within the uncertainty of the measurement.

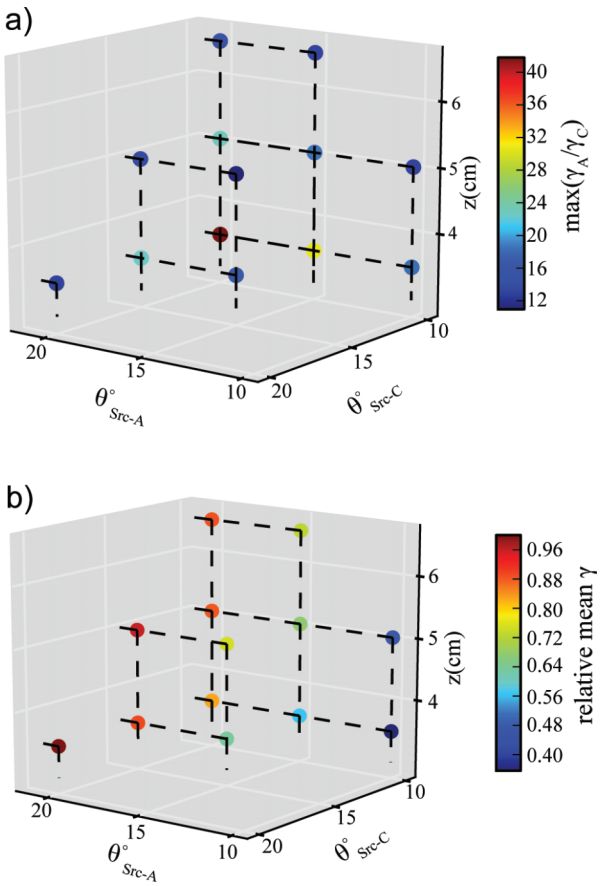

FIG. 6. Plots showing the maximum value of γ_A/γ_C (a) and relative mean total deposition rate (b) as a function of tilt angles for sources with elements "A" and "C" (θ_{Src-A} and θ_{Src-C}, respectively), and z. Deposition geometries with max(γ_A/γ_C) > 10 are shown. The dashed lines are added to assist the reader in identifying the coordinates of each data point.

III. RESULTS AND DISCUSSION

The deposition rates (γ) of Cu as a function of source tilt and x, y, z coordinates of the QCM are shown in Figure 3. With increasing source tilt angle (θ), the deposition rate increases over the entire x-y-z space, but the dynamic range ($\gamma_{max}/\gamma_{min}$) of deposition rate decreases, limiting the composition gradient that can be attained in co-deposition. Due to the orientation of the source with respect to the substrate, the deposition profile is symmetric about the y-axis, and the deposition gradient is larger along the x-axis compared to the z-axis. The gradient along the x-axis changes with both z and θ, allowing the user to choose appropriate values of these parameters to attain the desired deposition gradient across the substrate. The dynamic range of γ as a function of θ and z is shown in Fig. 4 and increases with decreasing z. For a given z, the dynamic range decreases as θ increases except at z = 3.5 cm, where the proximity of the substrate and source shifts the tilt for maximum dynamic range to θ = 15°.

Deposition profiling of individual sources provides requisite data for calculating the compositional coverage of a co-deposited film. For the purpose of illustrating the design of ternary compositional libraries, we consider co-deposition from 3 sources with elemental targets "A," "B," and "C." The three sources are placed symmetrically around the substrate with 120° in-plane separation. For simplicity, we assume

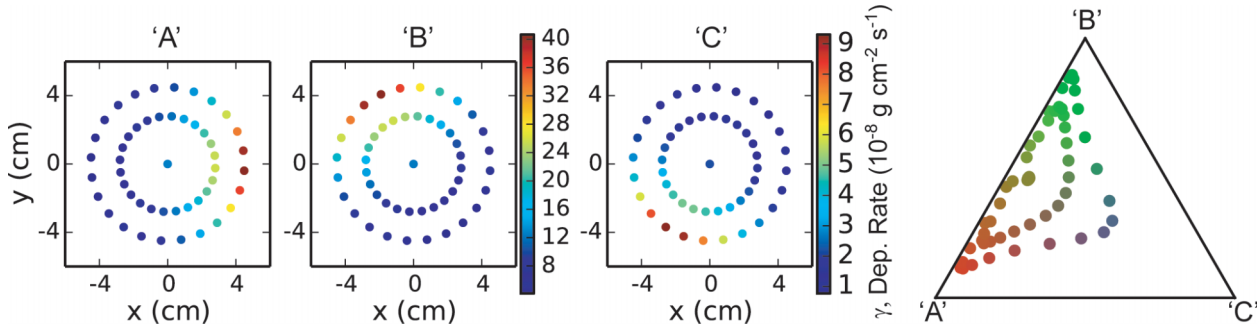

FIG. 7. Deposition rates of Cu at 60 W DC power and 0.8 Pa Ar from three sources tilted at $\theta_{Src-A} = 25°$, $\theta_{Src-B} = 25°$, $\theta_{Src-C} = 10°$, and z = 3.5 cm. The resulting compositions of the 49 measurement locations are shown in the right-most figure. This geometry results in a low concentration value of 2% for the alloying element "C".

that the deposition profile from each of the three sources is represented by the deposition profile of Cu shown in Fig. 3.

Let us now consider a deposition designed to cover a wide range of ternary compositions within a single thin film library. Maximal composition coverage is obtained by maximizing the dynamic range for each of the sources. Fig. 4 shows that dynamic range is maximized at θ = 15° and z = 3.5 cm; and using the 3-D deposition profiles shown in Fig. 3, the deposition rates and ternary composition coverage are shown in Fig. 5. Composition range of approximately 8%–82% is obtained for each element using this deposition geometry.

As a second demonstration of designing a synthesis experiment, consider the binary "A," "B" composition space in which the element "C" will be alloyed. For this purpose, it is desired to maximize the ratios γ_A/γ_C and γ_B/γ_C to provide a composition library that contains low concentrations of "C." For this application, we use the same tilt angles for sources A and B ($\theta_{Src-A} = \theta_{Src-B}$), and given the 3-source setup, the dynamic range of γ_A/γ_C and γ_B/γ_C are equivalent. In Fig. 6, we plot the maximum value of γ_A/γ_C and the total deposition rate of all 3 elements as a function of the free parameters of the deposition geometry θ_{Src-A}, θ_{Src-C}, and z. Only deposition geometries with a maximum value of γ_A/γ_C greater than 10 are plotted. To choose the best value among these geometry parameters, we consider the best compositional coverage that can be attained with a moderate to high deposition rate. The deposition geometry with $\theta_{Src-A} = 25°$, $\theta_{Src-B} = 25°$, $\theta_{Src-C} = 10°$, and z = 3.5 cm provides a maximum ratio of 42:1 for γ_A/γ_C (and for γ_B/γ_C) with a deposition rate that is 0.82 of the maximum deposition rate obtained among the various geometries.

The deposition rates for this selected deposition geometry, and the resulting composition coverage of the co-deposited library, are shown in Figure 7. This deposition geometry enables access to a composition of "C" as low as 2% over a wide range of ("A," "B") pseudo-binary compositions. A concentration as low as 2% cannot typically be accessed in co-sputtering when all three sources are in the same geometry due to limited ability to attain stable deposition at very low deposition rates. The low concentration of "C" desired in the ternary composition spread is attained by tailoring deposition geometries and sputtering rates.

IV. SUMMARY AND CONCLUSIONS

We present a custom combinatorial sputtering system with a new *in-situ* metrology employing an array of deposition rate monitors on a motorized stage. The instrument provides automated deposition profiling over a wide range of substrate positions and source tilt angles. These deposition profiles enabled a unique experimental design, as demonstrated through the optimization of deposition geometry for 2 types of ternary composition libraries. Beyond the experimental design, the deposition profiles provide a map of composition across a co-sputtered thin film, enabling measurement of composition-property relationships for high throughput combinatorial investigations.

ACKNOWLEDGMENTS

This manuscript is based upon work performed by the Joint Center for Artificial Photosynthesis, a DOE Energy Innovation Hub, supported through the Office of Science of the U.S. Department of Energy (Award No. DE-SC0004993). The authors thank Ryan R. J. Jones for assistance with chamber schematics, Frances Houle for insightful discussions, and Aniketa Shinde for assistance with the preparation of the manuscript.

[1]X. D. Xiang and I. Takeuchi, *Combinatorial Materials Synthesis* (Marcel Dekker, Inc., New York, 2003).
[2]K. Rajan, Annu. Rev. Mater. Res. **38**, 299 (2008).
[3]M. L. Green, I. Takeuchi, and J. R. Hattrick-Simpers, J. Appl. Phys. **113**, 231101 (2013).
[4]R. A. Potyrailo and E. J. Amis, *High Throughput Analysis: A Tool for Combinatorial Materials Science* (Kluwer Academic/Plenum Publishers, New York, 2003).
[5]J. N. Cawse, *Experimental Design for Combinatorial and High Throughput Materials Development* (John Wiley and Sons, New York, 2003).
[6]X. Liu, Y. Shen, R. Yang, S. Zou, X. Ji, L. Shi, Y. Zhang, D. Liu, L. Xiao, X. Zheng, S. Li, J. Fan, and G. D. Stucky, Nano Lett. **12**, 5733 (2012).
[7]Y. P. Deng, Y. F. Guan, J. D. Fowlkes, S. Q. Wen, F. X. Liu, G. M. Pharr, P. K. Liaw, C. T. Liu, and P. D. Rack, Intermetallics **15**, 1208 (2007).
[8]S. Guerin and B. E. Hayden, J. Comb. Chem. **8**, 66 (2006).
[9]S. Roncallo, O. Karimi, K. D. Rogers, J. M. Gregoire, D. W. Lane, J. J. Scragg, and S. A. Ansari, Anal. Chem. **82**, 4564 (2010).
[10]T. Iwasaki, N. Itagaki, T. Den, H. Kumomi, K. Nomura, T. Kamiya, and H. Hosono, Appl. Phys. Lett. **90**, 242114 (2007).
[11]J. S. Cooper and P. J. McGinn, J. Power Sources **163**, 330 (2006).
[12]S. Fujino, M. Murakami, V. Anbusathaiah, S.-H. Lim, V. Nagarajan, C. J. Fennie, M. Wuttig, L. Salamanca-Riba, and I. Takeuchi, Appl. Phys. Lett. **92**, 202904 (2008).

[13]J. R. Dahn, S. Trussler, T. D. Hatchard, A. Bonakdarpour, J. R. Mueller-Neuhaus, K. C. Hewitt, and M. Fleischauer, Chem. Mater. **14**, 3519 (2002).
[14]H. Chang, C. Gao, I. Takeuchi, Y. Yoo, J. Wang, P. G. Schultz, X.-D. Xiang, R. P. Sharma, M. Downes, and T. Venkatesan, Appl. Phys. Lett. **72**, 2185 (1998).
[15]X.-D. Xiang and P. G. Schultz, Phys. C: Supercond. **282-287**, 428 (1997).
[16]P. K. Schenck, N. D. Bassim, M. Otani, H. Oguchi, and M. L. Green, Appl. Surf. Sci. **254**, 781 (2007).
[17]D. Depla and W. P. Leroy, Thin Solid Films **520**, 6337 (2012).
[18]J. K. Bunn, C. J. Metting, and J. Hattrick-Simpers, JOM **67**, 154 (2015).
[19]J. M. Gregoire, R. B. van Dover, J. Jin, F. J. Disalvo, and H. D. Abruña, Rev. Sci. Instrum. **78**, 072212 (2007).
[20]J. M. E. Harper, J. Vac. Sci. Technol. **16**, 1901 (1979).
[21]J. M. Gregoire and R. B. van Dover, J. Vac. Sci. Technol., A **26**, 1030 (2008).
[22]T. Welzel, M. Kellermeier, K. Harbauer, and K. Ellmer, Appl. Phys. Lett. **102**, 211605 (2013).